

## Supporting Information

### Exploring the effects of different crystal facet combinations and I-doping in BiOCl/BiOI heterostructure on photocatalytic properties: A hybrid density functional investigation

Zuoyin Liu<sup>a</sup>, Bo Kong<sup>a\*</sup>, Xiang Xu<sup>a</sup>, Wentao Wang<sup>b\*</sup>

a. School of Physics and Astronomy, China West Normal University, Nanchong 637002, China;

b. Guizhou Provincial Key Laboratory of Computational Nano-Material Science, Guizhou

Education University, Guiyang, 550018, China;

\* Corresponding Authors, E-mail: xihuakb@163.com (B. K.); wuli8@163.com(W.W).

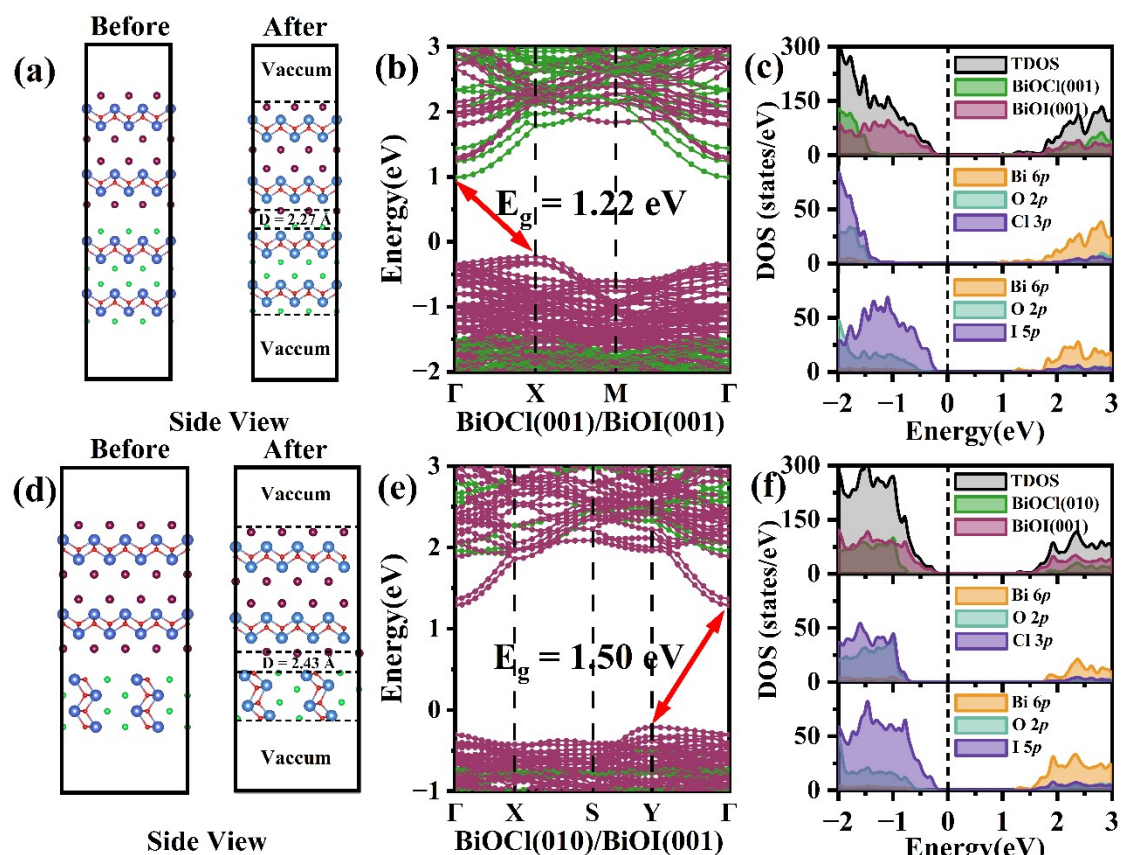


**Fig. S1.** Structural models (Sun et al.'s models in ACS Catalysis, 2015, 5(6), 3540-3551) before optimization and after optimization for (a) BiOCl(001)/BiOI(001), (d) BiOCl(010)/BiOI(001) heterostructures. The labelling of the atoms is the same as in Fig. 1. The projected band structures, TDOS and PDOS of (b-c) BiOCl(001)/BiOI(001) and (e-f) BiOCl(010)/BiOI(001) heterostructures; The green and brown lines represent the contribution from BiOCl and BiOI. The position of the Fermi energy level is set at 0 eV.

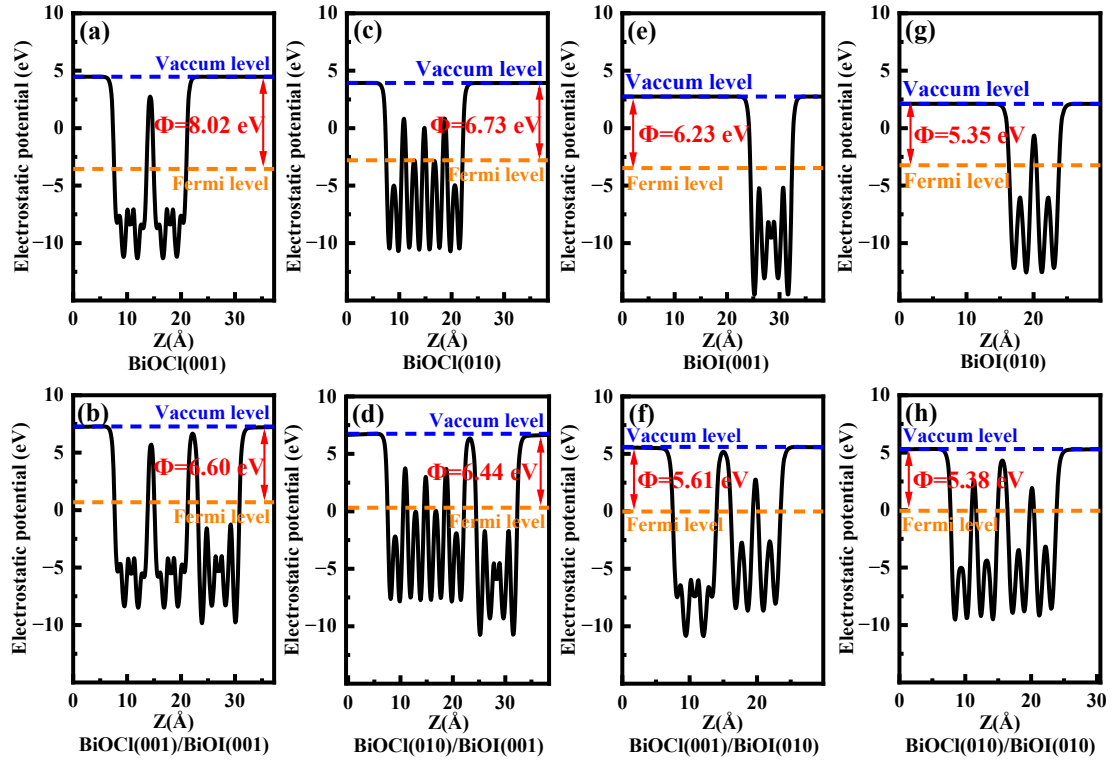


**Fig. S2.** Work functions of (a) BiOCl(001), (c) BiOCl(010), (e) BiOI(001) and (g) BiOI(010) sheets, and (b) BiOCl(001)/BiOI(001), (d) BiOCl(010)/BiOI(001), (f) BiOCl(001)/BiOI(010) and (h) BiOCl(010)/BiOI(010) heterostructures. The blue and orange lines denote the vacuum level and the Fermi level, respectively.

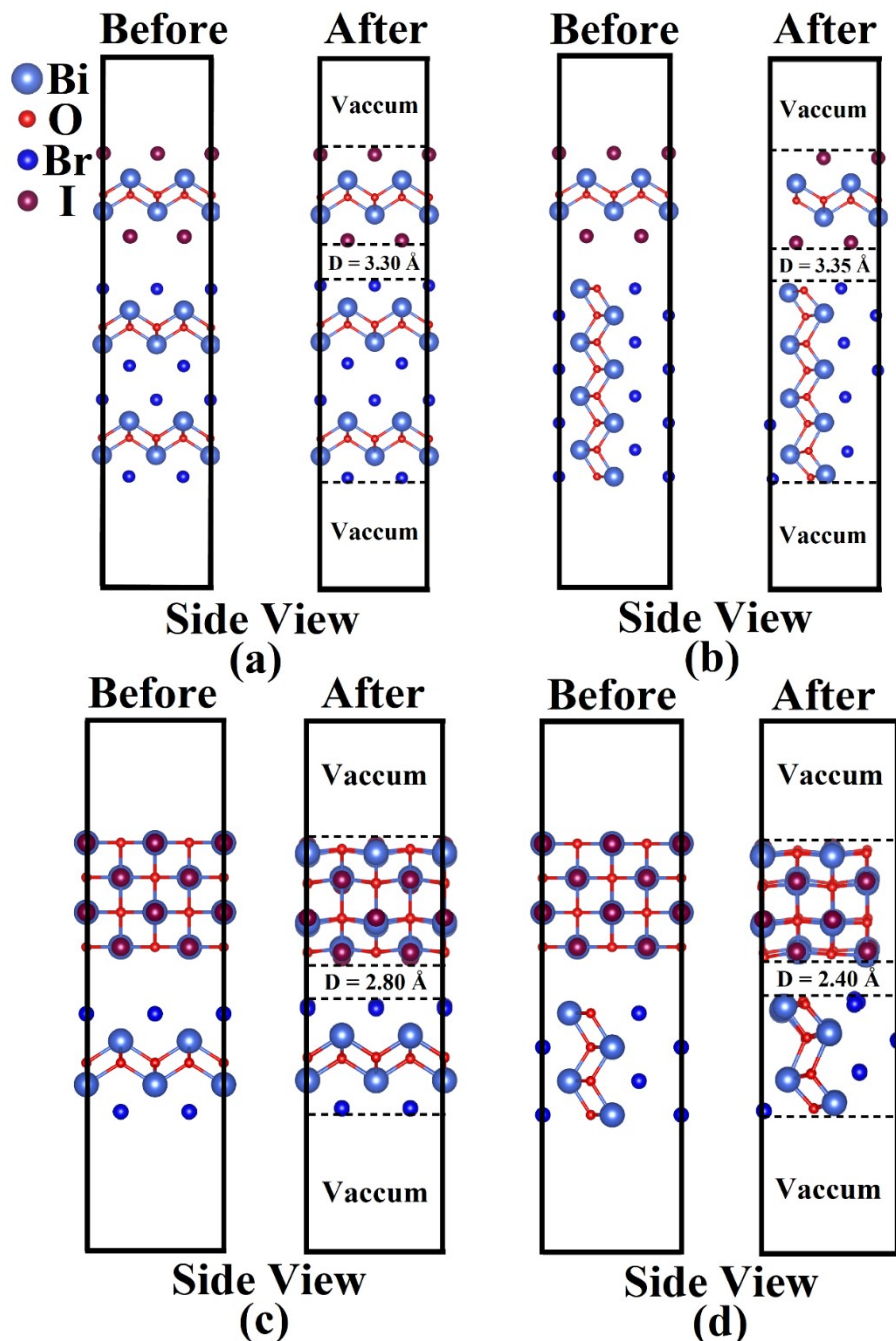


**Fig. S3.** Structural models before optimization and after optimization for (a) BiOBr(001)/BiOI(001), (b) BiOBr(010)/BiOI(001), (c) BiOBr(001)/BiOI(010) and (d) BiOBr(010)/BiOI(010) heterostructures.

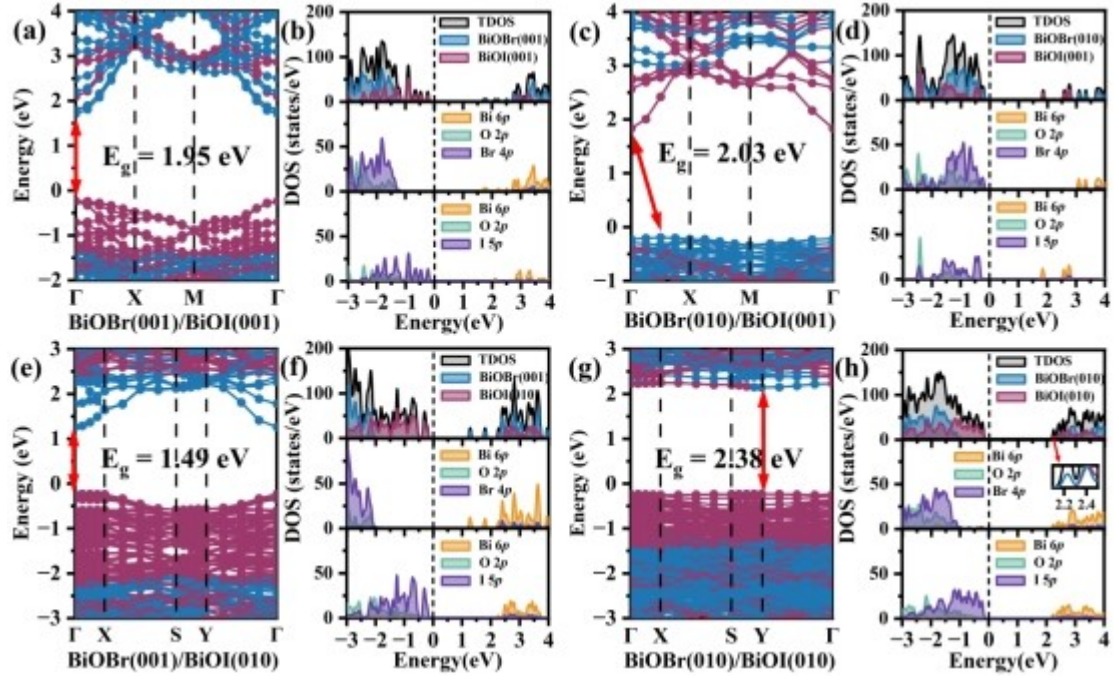


**Fig. S4.** The projected band structures, TDOS and PDOS of (a-b) BiOBr(001)/BiOI(001), (c-d) BiOBr(010)/BiOI(001), (e-f) BiOBr(001)/BiOI(010) and (g-h) BiOBr(010)/BiOI(010); The blue and brown lines represent the contribution from BiOBr and BiOI, respectively. The position of the Fermi energy level is set at 0 eV.

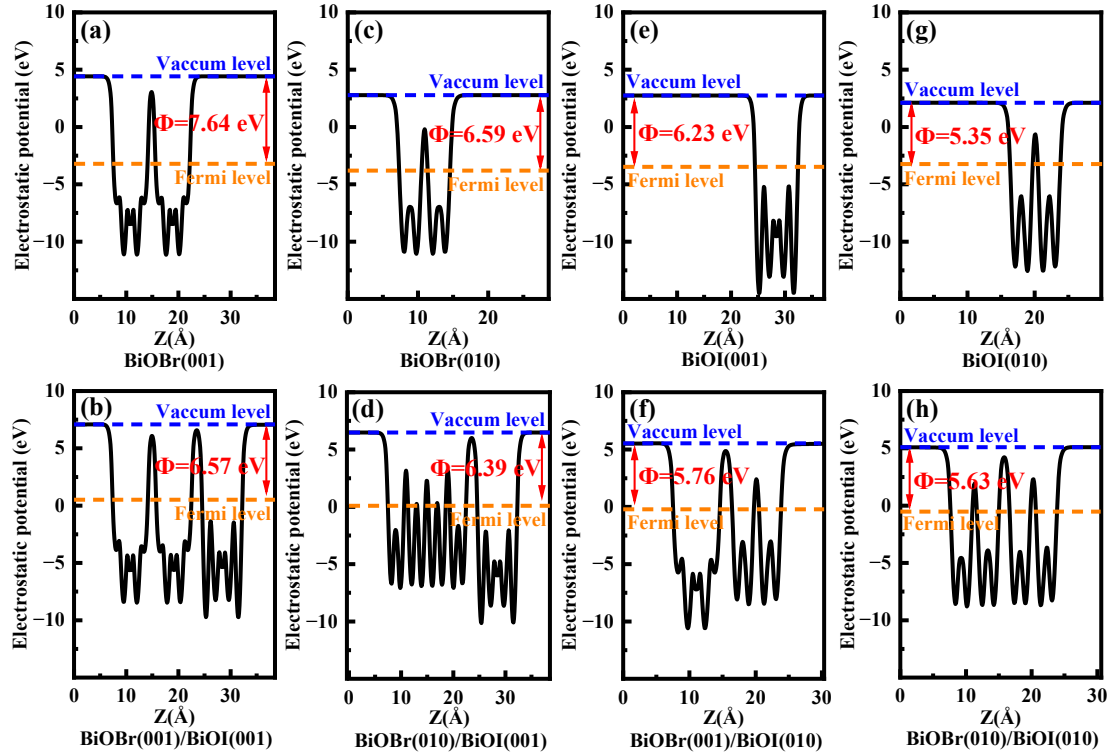


**Fig. S5.** Work functions of (a) BiOBr(001), (c) BiOBr(010), (e) BiOI(001) and (g) BiOI(010) sheets, and (b) BiOBr(001)/BiOI(001), (d) BiOBr(010)/BiOI(001), (f) BiOBr(001)/BiOI(010) and (h) BiOBr(010)/BiOI(010) heterostructures. The blue and orange lines denote the vacuum level and the Fermi level, respectively.

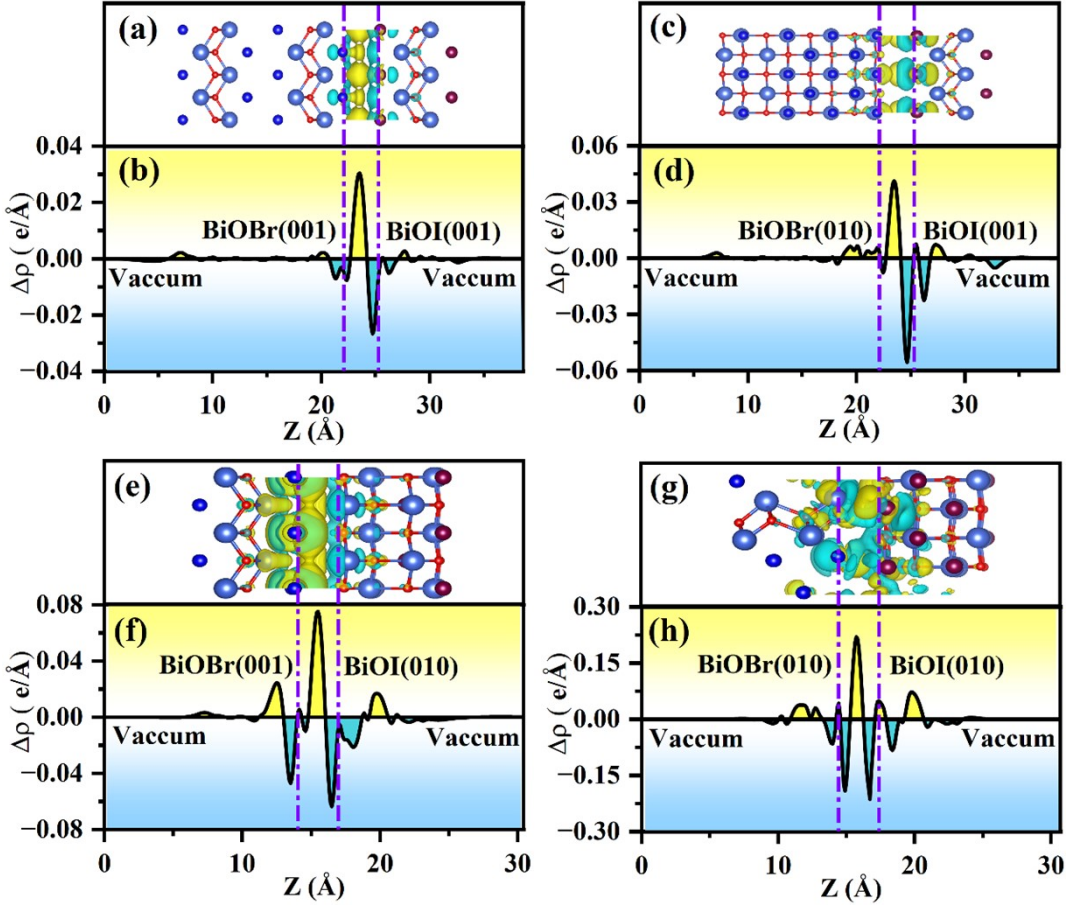


FIG. S6. The charge density difference and the planar-averaged differential charge density along with the Z direction of (a-b) BiOBr(001)/BiOI(001), (c-d) BiOBr(010)/BiOI(001), (e-f) BiOBr(001)/BiOI(010) and (g-h) BiOBr(010)/BiOI(010) heterostructures. The cyan region represents electron depletion, and the yellow region represents electron accumulation. The labelling of the atoms is the same as in Fig. S3.

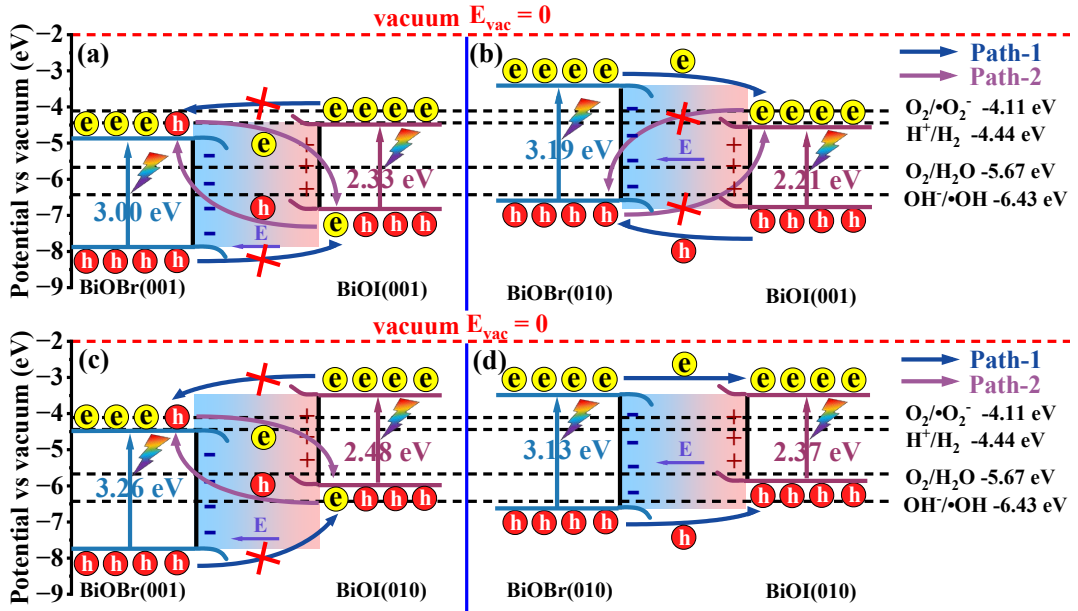
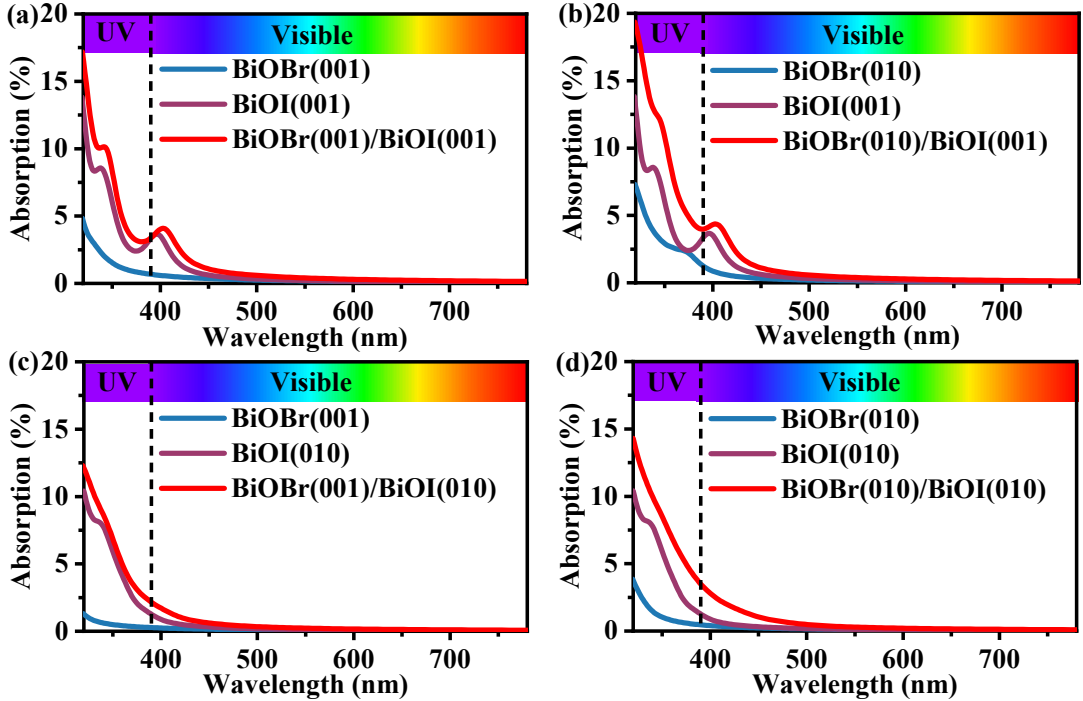
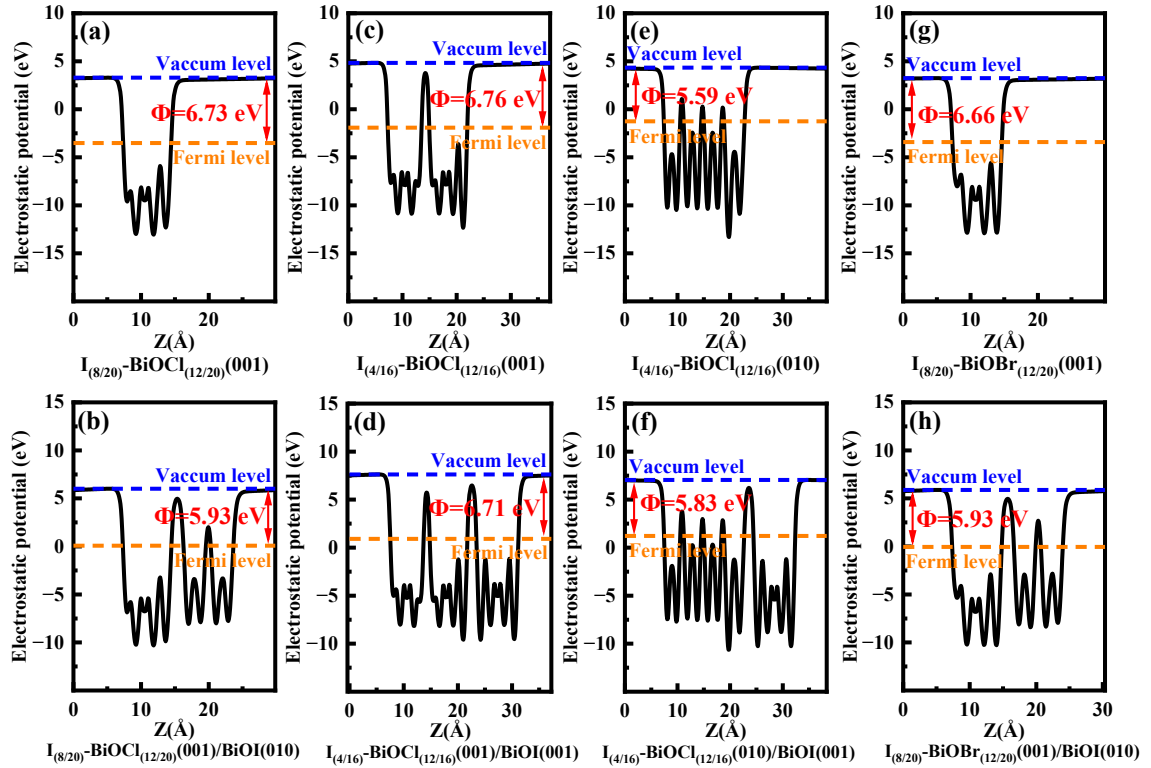


FIG. S7. The band alignment and charge separation at the interfaces of (a) BiOBr(001)/BiOI(001), (b) BiOBr(010)/BiOI(001), (c) BiOBr(001)/BiOI(010) and (d) BiOBr(010)/BiOI(010) heterostructures.



**FIG. S8.** Optical absorption spectra of isolated parts and their corresponding (a) BiOBr(001)/BiOI(001), (b) BiOBr(010)/BiOI(001), (c) BiOBr(001)/BiOI(010) and (d) BiOBr(010)/BiOI(010) heterostructures, respectively.



**Fig. S9.** Work functions of (a) I<sub>(8/20)</sub>-BiOCl<sub>(12/20)</sub>(001), (c) I<sub>(4/16)</sub>-BiOCl<sub>(12/16)</sub>(001), (e) I<sub>(4/16)</sub>-BiOCl<sub>(12/16)</sub>(010) and (g) I<sub>(8/20)</sub>-BiOBr<sub>(12/20)</sub>(001) sheets, and (b) I<sub>(8/20)</sub>-BiOCl<sub>(12/20)</sub>(001)/BiOI(010), (d) I<sub>(4/16)</sub>-BiOCl<sub>(12/16)</sub>(001)/BiOI(001), (f) I<sub>(4/16)</sub>-BiOCl<sub>(12/16)</sub>(010)/BiOI(001) and (h) I<sub>(8/20)</sub>-BiOBr<sub>(12/20)</sub>(001)/BiOI(010) heterostructures. The blue and orange lines denote the vacuum level and the Fermi level, respectively.

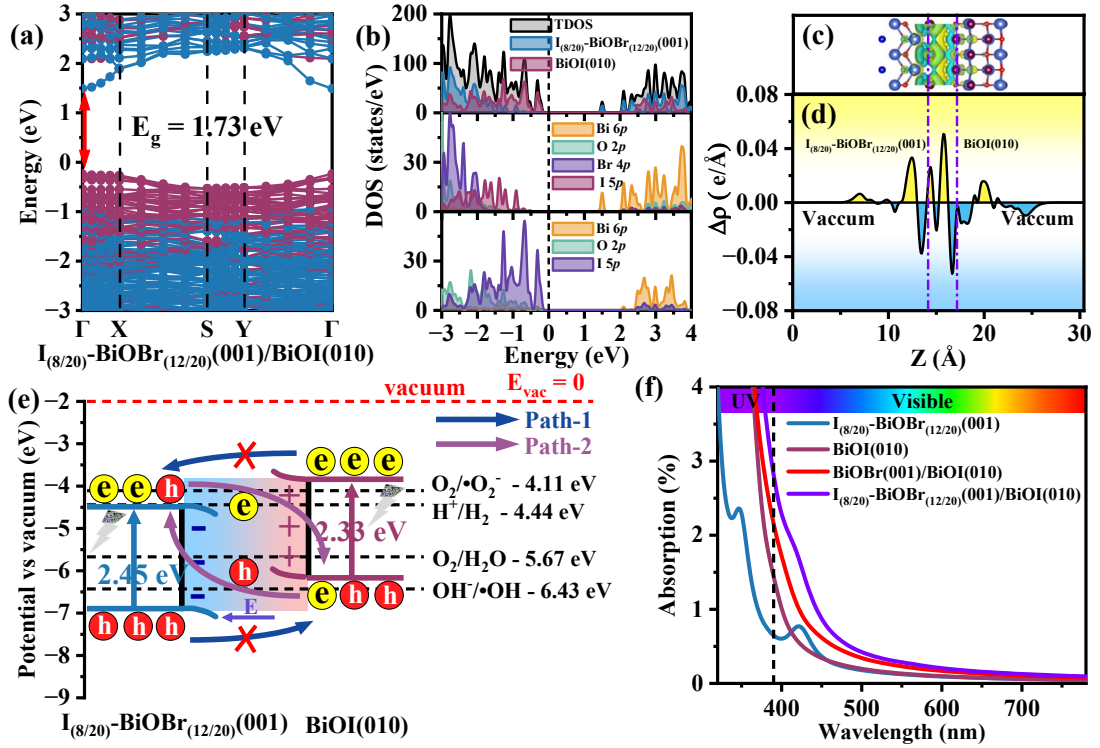


**Fig. S10.** The (a) projected band structure, (b) projected density of states, (c) charge density difference, (d) planar-averaged differential charge density along with the Z direction, and (e) band alignment of  $I_{(8/20)}\text{-BiOBr}_{(12/20)}(001)/\text{BiOI}(010)$  heterostructure. The (f) optical absorption spectra of  $I_{(8/20)}\text{-BiOBr}_{(12/20)}(001)$ ,  $\text{BiOI}(010)$ ,  $\text{BiOBr}(001)/\text{BiOI}(010)$  and  $I_{(8/20)}\text{-BiOBr}_{(12/20)}(001)/\text{BiOI}(010)$ .

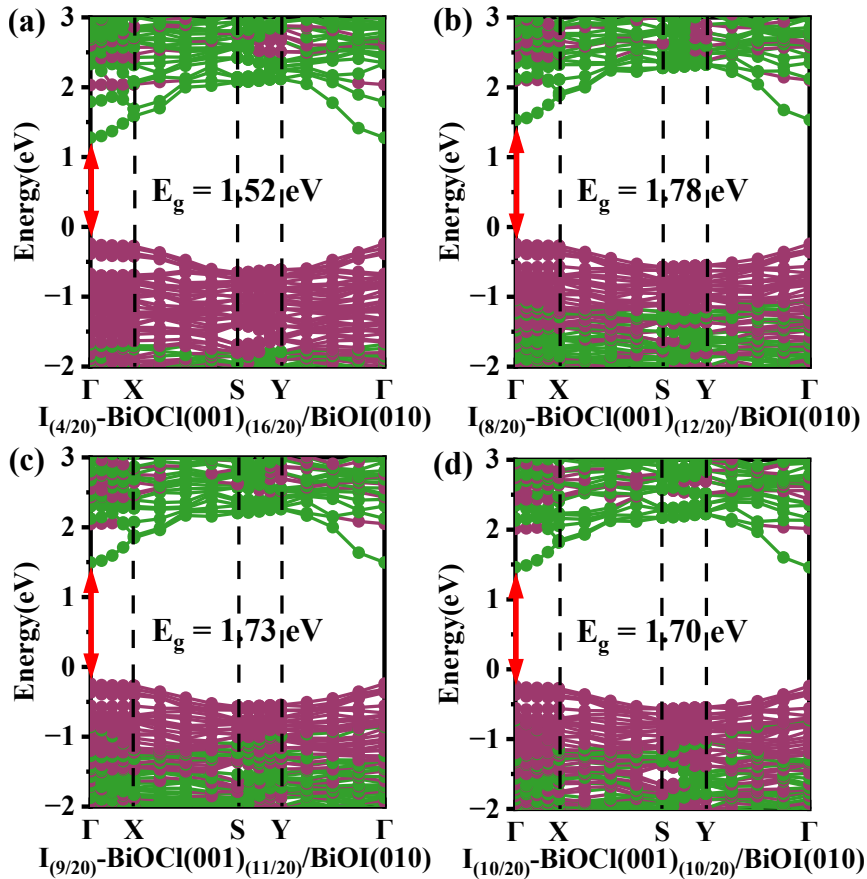


**Fig. S11.** The projected band structures, TDOS and PDOS of (a)  $I_{(4/20)}\text{-BiOCl}_{(16/20)}(001)/\text{BiOI}(010)$ , (b)  $I_{(8/20)}\text{-BiOCl}_{(12/20)}(001)/\text{BiOI}(010)$ , (c)  $I_{(9/20)}\text{-BiOCl}_{(11/20)}(001)/\text{BiOI}(010)$  and (d)  $I_{(10/20)}\text{-BiOCl}_{(10/20)}(001)/\text{BiOI}(010)$ ; The green and brown lines represent the contribution from BiOCl and BiOI, respectively. The position of the Fermi energy level is set at 0 eV.